Journal of Bacteriology

The Structure of the PapD-PapGII Pilin Complex Reveals an Open and Flexible P5 Pocket

Bradley Ford, Denis Verger, Karen Dodson, Ender Volkan, Maria Kostakioti, Jennifer Elam, Jerome Pinkner, Gabriel Waksman and Scott Hultgren

J. Bacteriol. **2012, 194(23):6390. DOI: 10.1128/JB.06651-11. Published Ahead of Print 21 September 2012.**

JB
Journals.ASM.org

The Structure of the PapD-PapGII Pilin Complex Reveals an Open and Flexible P5 Pocket

Bradley Ford,[a] Denis Verger,[c] Karen Dodson,[b] Ender Volkan,[b] Maria Kostakioti,[b] Jennifer Elam,[b] Jerome Pinkner,[b] Gabriel Waksman,[c] and Scott Hultgren[b]

Washington University Department of Pathology and Immunology[a] and Department of Molecular Microbiology and Center for Women's Infectious Disease Research,[b] St. Louis, Missouri, USA, and Institute of Structural and Molecular Biology, Birkbeck and University College London, London, United Kingdom[c]

P pili are hairlike polymeric structures that mediate binding of uropathogenic *Escherichia coli* to the surface of the kidney via the PapG adhesin at their tips. PapG is composed of two domains: a lectin domain at the tip of the pilus followed by a pilin domain that comprises the initial polymerizing subunit of the 1,000-plus-subunit heteropolymeric pilus fiber. Prior to assembly, periplasmic pilin domains bind to a chaperone, PapD. PapD mediates donor strand complementation, in which a beta strand of PapD temporarily completes the pilin domain's fold, preventing premature, nonproductive interactions with other pilin subunits and facilitating subunit folding. Chaperone-subunit complexes are delivered to the outer membrane usher where donor strand exchange (DSE) replaces PapD's donated beta strand with an amino-terminal extension on the next incoming pilin subunit. This occurs via a zip-in–zip-out mechanism that initiates at a relatively accessible hydrophobic space termed the P5 pocket on the terminally incorporated pilus subunit. Here, we solve the structure of PapD in complex with the pilin domain of isoform II of PapG (PapGIIp). Our data revealed that PapGIIp adopts an immunoglobulin fold with a missing seventh strand, complemented in parallel by the G1 PapD strand, typical of pilin subunits. Comparisons with other chaperone-pilin complexes indicated that the interactive surfaces are highly conserved. Interestingly, the PapGIIp P5 pocket was in an open conformation, which, as molecular dynamics simulations revealed, switches between an open and a closed conformation due to the flexibility of the surrounding loops. Our study reveals the structural details of the DSE mechanism.

Binding to surfaces is a critical first event that targets bacteria to specific niches and determines tropism. In Gram-negative bacteria, this interaction is frequently mediated by adhesins, present at the tips of both pilus and nonpilus fibers, which bind with stereochemical specificity to host cell surface ligands (67). These binding events are critical in the establishment of a foothold in a particular host tissue and can in some cases lead to internalization of the bacteria within host cells and initiation of host defense responses (40). For example, uropathogenic *Escherichia coli* (UPEC), the major causative agent of urinary tract infection (UTI) (15, 19), expresses type 1 pili which target UPEC to mannose epitopes in the bladder via the FimH adhesin located at their tip (8, 21, 38, 41). This event initiates a pathogenic cycle that involves binding, invasion, and the formation of intracellular bacterial communities, leading to acute and/or chronic cystitis (1, 29, 38, 40). Furthermore, over 90% of pyelonephritic *E. coli* strains produce P pili, which play a critical role in kidney infection through targeted interaction of the PapG tip adhesin with the globoseries glycolipids containing the Gal-α(1-4)-Gal disaccharide (11, 49, 50).

Type 1 pili (encoded by the *fim* operon) and type P pili (encoded by the *pap* operon) are assembled by chaperone/usher systems and are similar composite structures composed of rigid homopolymeric helical rods joined at their distal end to a heteropolymeric thin tip fibrillum containing a specific carbohydrate-binding adhesin (Fig. 1A) (20, 28, 33, 67). Chaperone/usher systems are nearly ubiquitous in Gram-negative organisms (67). Nuccio and Baumler identified 189 chaperone/usher systems in a wide variety of pathogens, including *Salmonella*, *Haemophilus*, *Klebsiella*, and *Yersinia* (43). Many of these systems assemble adhesive fibers involved in virulence (54, 59). Therefore, it is important to understand the molecular basis of the mechanism by which the chaperone/usher systems function.

Each chaperone/usher system consists of different polymerizing pilin subunits, a periplasmic chaperone, and an outer membrane usher, all of which are transported into the periplasm via the Sec machinery (32). There are two basic types of pilin subunits that give rise to the mature pilus: (i) single-domain subunits and (ii) two-domain tip adhesins, such as FimH and PapG, which localize at the tip of the pilus (67). Pilin subunits consist of a short (~11- to 17-amino-acid) **N**-**t**erminal **e**xtension (Nte) followed by an incomplete immunoglobulin (Ig)-like fold missing the C-terminal beta strand (8, 52, 67). This necessitates the presence of a periplasmic chaperone for subunit folding and stability once transported across the inner membrane (4, 5). The chaperones (~25 to 30 kDa) are highly homologous in structure and have a number of invariant and highly conserved amino acid residues (23, 67). Each chaperone consists of two Ig-like domains stabilized by a conserved salt bridge in an overall boomerang shape (18, 22). Two families of chaperones were observed on the basis of the length of the F1-G1 loop in the N-terminal domain (23). Chaperones with a **s**hort **F**1-**G**1 loop (FGS) were found to be involved in

Received 6 December 2011 **Accepted** 3 September 2012
Published ahead of print 21 September 2012
Address correspondence to Scott Hultgren, hultgren@borcim.wustl.edu.
B.F. and D.V. contributed equally to this article.
We dedicate this article to the memory of Denis Verger.
Supplemental material for this article may be found at http://jb.asm.org/.

doi:10.1128/JB.06651-11

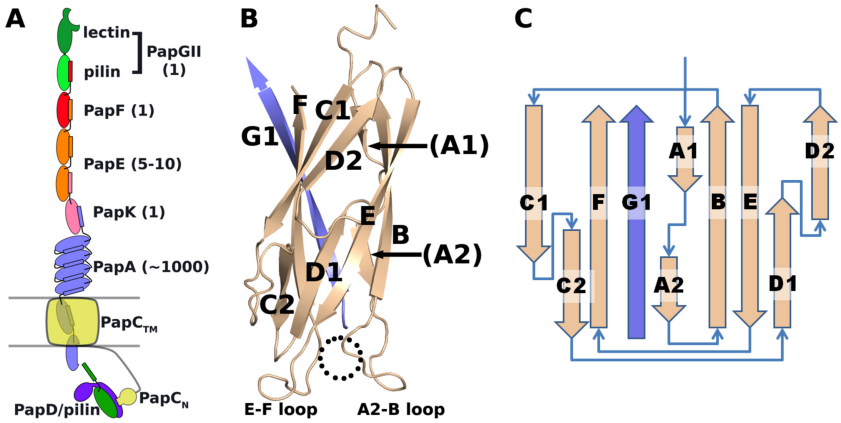

FIG 1 (A) P-pilus schematic with stoichiometry of subunits in parentheses. The PapGII pilin domain is in light green. The PapC usher in yellow is represented by transmembrane (TM) and N-terminal (N) domains (its plug domain and C-terminal domain are omitted). The periplasmic PapD chaperone is in purple and is bound to a pilin domain, as in the PapD-GIIp complex structure shown in panel B. (B) PapD/GIIp structure, with the blue G1 strand of the chaperone complementing the tan pilin domain. The P5 pocket is outlined by the dotted circle. The full-length two-domain PapD protein was crystallized with PapG; only the PapD G1 structure, which is the chaperone domain that interacts with the pilin subunit, is shown for clarity. (C) Topology diagram of the complex in panel B. Loops are named after the strand that they connect.

the assembly of fibers that possess a thick rod comprised of subunits arranged in a helical cylinder (23, 67). Chaperones with a **l**ong **F**1-**G**1 loop (FGL) assembled nonpilus fibers that consist of either simple oligomers or amorphous fibers (58, 67, 70). The crystal structures of several FGS chaperones have been solved, including PapD (18), FimC (45), and SfaE (31), as have the two FGL chaperones Caf1M (70) and SafB (47). The periplasmic chaperones function to fold their corresponding subunits and shield interactive subunit surfaces in the periplasm, in a process that we termed donor strand complementation (DSC) (5, 8, 27, 52, 56). The active site of each chaperone contains a conserved subunit binding site consisting of (i) two positively charged cleft residues (R8 and K112 in PapD) that hydrogen bond to the COOH terminus of their target subunits and (ii) solvent-exposed hydrophobic residues extending up the G1 strand of domain 1 from the cleft of the chaperone that participate in DSC (24, 34, 58). Chaperone-subunit complexes are targeted to an outer membrane usher that serves as a platform for pilus assembly and secretion across the outer membrane (32, 42, 48, 52, 56, 67).

During incorporation into the growing pilus, the Nte of each pilin subunit is capable of replacing the donor strand contributed by the chaperone during a process of **d**onor **s**trand **e**xchange (DSE) (47, 53). In DSE, a hydrophobic P5 residue on the Nte of the next incoming subunit inserts into the corresponding unoccupied P5 pocket on the terminal subunit, initiating a zip-in–zip-out reaction in which DSE propagates through the P4, P3, P2, and P1 pockets, displacing chaperone residues occupying these pockets during DSC (6, 47, 69). This process is catalyzed by the outer membrane usher, which has been shown to differentially bind chaperone-subunit complexes (10, 56, 66).

In the case of P pili, the PapG adhesin localizes at the distal end of the tip fibrillum. There are three classes of PapG adhesins with different lectin binding preferences. Various glycolipid binding assays have been used to distinguish PapG adhesins belonging to three different classes (classes I, II, and III) (61). All three classes recognize Galα-4Gal-containing glycolipids but with different stereochemical specificities, depending on neighboring carbohydrates. The class I adhesin recognizes globotriaosyl ceramide (GbO_3), whereas class II binds globotetraosyl ceramide (GbO_4) and class III recognizes the Forssman glycolipid with a terminal GalNAc (GbO_5). Isoform II of PapG (PapGII) is the most common form of adhesin found in UPEC isolates causing pyelonephritis in humans (11). PapF adapts PapG to the pilus tip and also plays a role in initiating pilus assembly (35). PapE interacts with PapF's Nte, and multiple PapE monomers make up the bulk of the open helical tip fibrillum (37, 60). PapK adapts the tip fibrillum to the pilus rod via interactions with PapA's Nte (25). Repeating monomers of PapA arranged in a right-handed helical cylinder form the homopolymeric pilus rod (3, 14, 63). PapA and PapE Ntes are able to complete the fold of other PapA and PapE Ig-like domains, respectively, allowing formation of linear homopolymers (14, 51). In the case of PapA, surfaces on pilin then engage in further interactions that promote the coiling of the linear PapA fiber into a rigid helical rod consisting of ~3.3 PapA subunits per turn (14). The Nte of PapH interacts with PapA, and incorporation of PapH terminates pilus assembly and thus regulates the length of the pilus rod (2, 64).

The catalysis and assembly of the subunits into the mature pilus occur at the outer membrane assembly platform, PapC, upon ordered delivery of subunits by the chaperone, PapD (16, 62, 66, 67). The PapC usher contains five functional domains: a transmembrane beta barrel, a beta sandwich plug, an N-terminal periplasmic domain (NTD), and two C-terminal periplasmic domains (CTD1 and -2). During pilus assembly, subunits dock as chaperone-bound complexes to the usher, which catalyzes their polymerization and mediates pilus translocation across the outer membrane (42). The plug domain occludes the pore of the transmembrane domain of a solitary usher, but the chaperone-adhesin-bound usher has its plug displaced from the pore, adjacent to the NTD (46, 66). An interaction between the NTD and plug domains suggested a biophysical basis for usher gating (66). The plug-NTD surface subsequently actively recruits chaperone-subunit complexes to the usher. CTD2 has a catalytic role in transferring the chaperone-adhesin complex from NTD to CTD2 during pilus initiation (46, 66). Thus, the growing pilus structure in which each seven-stranded Ig fold pilin domain is made up of six

strands (strands A to F) of one subunit and the Nte of the next pilin subunit is translocated across the outer membrane usher (10, 48, 55). This results in a highly stable pilus structure.

Previously, we have solved the structures of PapD-PapK (52), PapD-PapE (53), PapD-PapA (63), PapD-PapH (64), and PapD-PapF (65). In this study, we present the crystal structure of the remaining chaperone-pilin structure of the P-pilus system: PapD bound to the pilin domain of isoform II of the PapG adhesin (PapGIIp). The PapGIIp structure revealed an immunoglobulin fold with a missing seventh strand interacting in parallel with the G1 strand of the chaperone. Comparisons between PapD-GIIp and the other PapD-pilin structures indicate that while the PapD chaperone interacts with each of the pilins in conserved ways to promote pilin folding and stability, the subunit surfaces that bind to the chaperone are not identical in their amino acid sequence. However, analyses of these structures illustrate a high level of conservation in PapD-pilin interactions. Surprisingly, although previous *in vitro* studies had shown a low DSE rate between PapG and the adjacent PapF pilin, suggestive of an obstructed PapG P5 pocket (51), the PapGIIp structure revealed an open pocket conformation. Molecular dynamics simulations of the PapD-GIIp structure assessing the P5 pocket accessibility illustrate that the PapGIIp P5 pocket is highly flexible, switching between an open and a closed state within 12 ns due to shifting of the surrounding A2-B and E-F loops. These studies suggest a higher rate of DSE than has previously been reported *in vitro* for PapG and PapF and imply that additional factors besides the P5 pocket determine the rate of DSE *in vivo*. Thus, the solved PapD-GIIp crystal structure provides further insights into the DSE mechanism and the role of the usher in this process that may enhance our understanding of the assembly of these virulent organelles by Gram-negative pathogens.

MATERIALS AND METHODS

Construct generation and expression. For crystal form 1, *papD* was cloned into pMMB91 as described by Slonim et al. (58). The 6His-PapGIIp construct was made using standard PCR recombinant techniques and plasmid pDC1 (9), which carries the full-length *papGII*, as the template. A 6His tag was inserted in place of the PapGII lectin domain between the PapGII signal sequence and the pilin domain of PapGIIp; this results in a mature N terminus of the recombinant protein containing 6 histidines followed by the pilin domain. No modifications were made to the C terminus of PapGII. The resulting 6His-PapGIIp was inserted into the pTryc vector (68), an isopropyl-β-D-thiogalactopyranoside (IPTG)-inducible chloramphenicol-resistant derivative of pTrc99a (Invitrogen Inc.). The resulting constructs were transformed into *E. coli* DL41, a methionine auxotroph.

For crystal form 2, *papD* was cloned by PCR from *E. coli* UTI89 genomic DNA using oligonucleotides flanked by BamHI and XbaI restriction sites and described elsewhere (60). *papGII* was extracted from plasmid pDC1 (9). The *papD* and *papGII* genes were introduced into the pTrc99A plasmid (Invitrogen Inc.) by a 3-point ligation, resulting in pTRC-DGII. In order to design the 6His-PapGIIp, the coding sequence for 6 histidines was used to replace the PapGII lectin domain in pTRC-DGII as described above. No modifications were done at the C terminus of the PapGII protein. The resulting construct, pTRC-DGII$_{His}$, was transformed into *E. coli* C600 cells.

C600 cells were grown in Terrific broth (Sigma, Inc.), whereas DL41 cells were grown in minimal medium containing all amino acids but with selenomethionine instead of methionine. Cells were grown under shaking conditions in a 5-liter fermentor vessel at 37°C in the presence of corresponding antibiotics. At an optical density at 600 nm of 0.9, cells were induced with 1 mM IPTG and kept growing for another 3.5 h. Cells were pelleted, and the PapDGII$_{His}$ complex was extracted from the cell periplasm as previously described (10).

Crystallization and data collection of the two PapD-GIIp forms. The PapD-GIIp form 1 complex was purified on a cobalt affinity column (Talon; Clontech), followed by a Q Sepharose column (Source 15Q; GE Healthcare) and dialysis against 20 mM morpholineethanesulfonic acid (MES) buffer, pH 6.5. The complex was crystallized by the hanging-drop vapor diffusion method by mixing 2 μl protein complex at 15 mg/ml in 20 mM MES, pH 6.5, with 2 μl mother liquor. The best crystals were obtained at 20°C with mother liquor consisting of 1 M sodium malonate, pH 7.3. Sorbitol was added to 25% as cryoprotectant. X-ray diffraction data were collected from a single flash-cooled crystal (−180°C) at beamline 4.2.2 of the Advanced Light Source (Berkeley, CA). The data were processed with the MOSFLM program (36) and scaled with the SCALA program (30). Selenium single anomalous dispersion (Se-SAD) phasing (12) and heavy-atom location were performed in a Phaser EP apparatus (39) after location of the heavy atoms by the SHELXD program (57). The model was refined with the REFMAC program; TLS (translation, libration, screw-rotation) refinement was performed using groups determined by the TLSMD server. Water molecules were initially added to a spherical density at 3.0 sigma in an $F_o - F_c$ map (where F_o is the observed structure factor and F_c is the structure factor of the modeled structure) and were retained in the final model if they occupied a density above 0.8 sigma in a $2F_o - F_c$ map, were at least 2.2 Å from protein atoms, and were not more than 3.4 Å from protein atoms. Data collection and refinement statistics are summarized in Table 1.

The PapD-GIIp form 2 complex was purified on a cobalt affinity column (Talon; Clontech), followed by a phenyl-Sepharose column (Source; GE Healthcare) and dialysis against 20 mM Tris-HCl buffer, pH 7.5, 20 mM NaCl. The complex was crystallized by the hanging-drop vapor diffusion method by mixing 1 μl protein complex at 9.9 mg/ml in 20 mM Tris-HCl, pH 7.5, 20 mM NaCl with 1 μl mother liquor. The best crystals were obtained at 20°C with mother liquor consisting of 10% polyethylene glycol (PEG) 4000, 0.1 M Tris HCl, pH 8.5, and 5% isopropanol. An additional 25% PEG 400 was added as a cryoprotectant. X-ray diffraction data were collected from a single flash-cooled (−180°C) crystal at beamline ID 23_2 of the ESRF (Grenoble, France). The structure was solved by molecular replacement, using the PapD-PapK complex (Protein Data Bank [PDB] accession number 1PDK) as the search model with the program AMoRe. The model was refined with a crystallography and nuclear magnetic resonance system (CNS). Successive cycles of manual rebuilding with O and conjugate gradient minimization using CNS were performed. B factors (the temperature factor, where B_i equals $8\pi^2 Ui^2$ and Ui^2 is the mean square displacement of atom i) were refined individually. Water molecules were added in agreement with expected hydrogen bond distances and an $F_o - F_c$ density greater than or equal to 3.5 sigma. Data collection and refinement statistics are summarized in Table 1. Given that the diffraction limit was lower for PapD-GIIp form 2 and because no appreciable differences were observed between the two PapD-GIIp forms, we have used the higher-resolution PapD-GIIp form 1 for all chaperone-pilin comparisons described in this report.

Molecular dynamics simulations. Simulations were performed using the GROMACS (version 4.0.2) program (17) at 310 K and explicit SPC/E (single point charge/extended) water with Na^+ and Cl^- ions added to neutralize the charge and simulate a physiological salt concentration of 150 mM. The crystallographic complex of PapD-GIIp (PDB accession number 3MEO) was used with structural water molecules, and the six-histidine tag was removed. The PapGIIp-PapF complex was modeled used pilin domain models from crystallographic PapD complexes (PDB accession numbers 3MEO and 2W07, respectively), with the pilin domains initially superposed on those of the PapA dimer in the crystallographic PapA$_{DSE}$ complex (PDB accession number 2UY6). The Nte of PapF was also modeled on that of the PapA$_{DSE}$ complex, and structurally absent loops were modeled and their geometry was corrected in the COOT pro-

TABLE 1 Data collection and refinement statistics

Parameter[a]	Value for[b]: Selenomethionine PapD-GIIp-His[c]	Native PapD-GIIp-His[d]
Data collection statistics		
Wavelength (Å)	0.9790	0.8726
Space group	$P2_12_12$	$P2_12_12$
No. of PapD-PapGIIp complexes in asymmetric unit	1	1
Solvent content (%)	43.8	44.8
Cell dimensions		
a, *b*, *c* (Å)	103.7, 65.8, 56.5	66.6, 90.5, 64.5
α, β, γ (°)	90.0, 90.0, 90.0	90.0, 90.0, 90.0
R_{merge}	10.8 (52.6)	13.0 (50.0)
$I/\sigma[I]$	23.9 (5.7)	13.2 (3.9)
Completeness (%)	99.7 (97.7)	100.0 (100.0)
Redundancy	14.0 (12.3)	6.6 (6.7)
R_{merge}	0.108	0.130
Refinement statistics		
Resolution range (Å)	28.4–2.0 (2.08–2.03)	66.6–2.3 (2.42–2.30)
No. of reflections	24,169	17,935
R_{work}/R_{free}	0.182/0.190	0.227/0.289
No. of atoms		
Total (non-H)	3,015	2,543
Water molecules	314	192
Mean overall B factor	27.6	33.2
RMSDs		
Bond length (Å)	0.022	0.006
Bond angles (°)	1.114	1.318
Ramachandran plot[e]		
% most favored residues	94.7	94.9
% additional favored residues (outliers)	3.8 (1.5)	3.0 (2.1)

[a] $R_{merge} = \sum_{i,hkl}|\langle I(hkl)\rangle - I_i(hkl)|/\sum_{i,hkl}I_i(hkl)$, where I_i is the *i*th intensity measurement of a reflection of Miller index *hkl* and $<I>$ is the average intensity from multiple observations; $R_{work} = \sum_{(hkl)\in W}||F_o| - |F_c||/\sum_{(hkl)\in W}|F_o|$, where *W* is the working set; $R_{free} = \sum_{(hkl)\in T}||F_o| - |F_c||/\sum_{(hkl)\in T}|F_o|$, where *T* is the test set obtained by randomly selecting 5% of the data.

[b] Values in parentheses are for the highest-resolution shell.

[c] Form 1 (selenomethionine PapD-GIIp-His) data were collected at beamline 4.2.2 at the Advanced Photon Source, Berkeley, CA.

[d] Form 2 (native PapD-GIIp-His) data were collected at beamline ID 23_2 at ESRF, Grenoble, France.

[e] Calculated with the RAMPAGE program (30).

gram (13), before energy minimization and a 150-ps equilibration run, during which protein atoms were held static.

The dynamics of the PapD-GIIp complex were simulated for 20 ns (see Fig. 4), while the GIIp-PapF complex was simulated over a 1-ns production run during which an energy minimum was achieved (see Fig. 3).

Protein structure accession numbers. Crystal form 1 coordinates and structure factors have been deposited in PDB under accession number 3ME0; crystal form 2 coordinates and structure factors have been deposited in PDB under accession number 2WMP.

RESULTS

Conserved features of PapD in complex with GIIp. We determined the structure of PapD in complex with the PapGII pilin domain (PapGIIp) under two different crystallization conditions (here referred to as form 1 and form 2). Form 1 was used for all comparisons described below since it diffracted to a higher resolution. While these two forms exhibit differences from one another and with other PapD-pilin complexes (discussed below), they share all conserved interactions with PapD. The root mean square deviation (RMSD) between form 1 and 2 crystal structures is 1.32 Å. We first compared PapD-GIIp to other PapD-pilin complexes with respect to both conserved structural elements and PapD-pilin interactions. The overall fold of PapGIIp is that of an immunoglobulin fold with a missing seventh strand that is complemented by the parallel G1 strand of PapD (Fig. 1B and C; see Fig. S1 in the supplemental material). This is similar to that of known complexes of PapD with the pilin domains PapK (PDB accession number 1PDK) (52), PapE (PDB accession number 1N0L) (53), PapH (PDB accession number 2J2Z) (64), PapA (PDB accession number 2UY6) (63), and PapF (PDB accession number 2W07) (65). In the PapA structure, one pilin domain is donor strand complemented through binding to PapD (here referred to as $PapA_{DSC}$), and this pilin domain is joined through its Nte to a donor-strand-exchanged PapA pilin domain (here referred to as $PapA_{DSE}$) (63). Comparison of these two domains illustrates the subtle changes that pilin domains undergo during DSE.

TABLE 2 RMSD between pilin domains following secondary-structure matching (SSM) superposition in COOT

Pap	RMSD (Å): PapA (DSE)	PapA (DSC)	PapE	PapF	PapGIIp	PapH	PapK
PapA (DSE)	0.00	1.59	2.18	2.29	2.01	2.00	1.99
PapA (DSC)		0.00	1.97	2.13	2.94	1.76	2.13
PapE			0.00	2.06	2.59	2.18	2.19
PapF				0.00	2.01	2.02	2.23
PapGIIp					0.00	2.87	2.86
PapH						0.00	1.91
PapK							0.00

Between pilin domains in complex with PapD (with the exception of $PapA_{DSC}$), the RMSD over all alpha-carbon atoms ranges from a deviation of 1.59 Å between $PapA_{DSC}$ and $PapA_{DSE}$ to the largest deviation (2.94 Å) between PapGIIp and $PapA_{DSC}$ (Table 2). The lowest RMSD between PapGIIp and another pilin domain is 2.01 Å for both $PapA_{DSE}$ and PapF. PapF and PapGIIp share a closely aligned beta-sheet core but differ significantly in the conformation of connecting loops. Significant deviations between PapGIIp and PapF occur in the F-E and A2-B loops that surround the P5 pocket and in a shorter D1-D2 loop in PapGIIp relative to other Pap pilin domains. PapGIIp shares an extended B-C1 loop with PapF relative to other pilin domains. Both crystal forms share essentially all features discussed above. PapA deviates from PapGIIp more significantly in the core fold.

Across all PapD-pilin complexes, there are only minor differences in the conformation of PapD, with the overall RMSD ranging from 0.54 to 0.92 Å. Differences in the conformation of PapD between the PapD-GIIp structure and other PapD-pilin complexes include changes at Tyr197 of PapD, which is rotated ~180° relative to the PapD-PapF, PapD-PapE, and PapD-PapH structures. In PapD-GIIp, Tyr197 makes a 2.74-Å hydrogen bond with the GIIp backbone nitrogen of Gly215. In the PapD-PapF and PapD-PapE structures, this space is occupied instead by the side chain of a hydrophobic residue (Ile12 and Val1 of PapF and PapE,

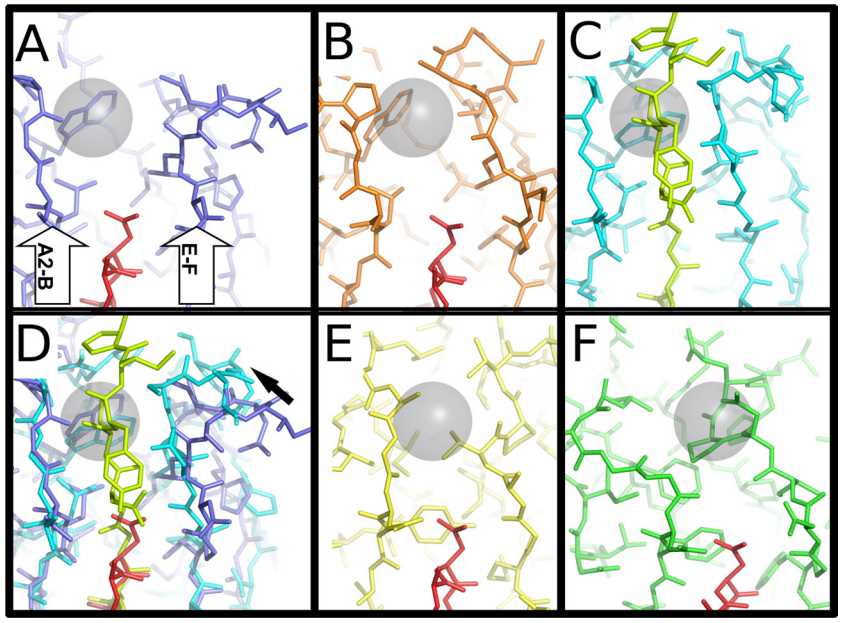

FIG 2 P5 pockets, illustrated by a translucent sphere centered on the carbon beta of the P5 residue of the PapF donor strand bound to PapG, modeled through molecular dynamics simulation (C) (see text). In all cases, the P5 pocket is flanked by the A2-B loop on the left and the E-F loop on the right (labeled in panel A). (A and B) The P5 pocket in the crystallographic form 1 PapD-PapGII complex (A) and the form 2 complex (B). (D) The form 1 complex at the start (blue) and end (teal) of the molecular dynamics simulation of the PapF (donor strand in yellow)-PapG complex. Black arrow, the shift of the E-F loop from the crystallographic conformation. (E and F) There is no P5 pocket in PapH (PDB accession number 2J2Z) (E) and an obstructed P5 pocket in PapF (PDB accession number 2W07) (F).

respectively). In the PapD-PapH structure, the conformation of Tyr-197 found in PapD-GIIp is obstructed by a 30° rotation of the free N-terminal extension of the pilin domain. In the PapD-$PapA_{DSE}$ complex, the terminal donor-strand-complemented pilin domain occupies the space occupied by Tyr197 in the PapGIIp structure. Finally, in the PapD-PapK structure, the 110° angle formed by the Nte with the body of the pilin domain occurs 1 amino acid closer to the invariant cysteine residue at the C terminus of the Nte due to the presence of a proline residue at position 13. Whether these differences in structure contribute to the specificity of DSE is not clear in the absence of structures of donor-strand-exchanged pilin domains.

The interaction of PapD with the range of pilin domains is essentially static across the PapD residues that interact with the P2, P3, and P4 pockets of the pilin domains, with the exception of Leu107 of PapD, which occupies the P2 pocket. It exhibits one rotameric form in complex with PapA, PapE, and PapH and another in complex with PapGIIp, PapF, and PapK. The conformation of PapD's Leu107 in the PapD-GIIp complex is sterically excluded by an isoleucine in PapA, leucine in PapH, and valine in PapE at the position equivalent to residue 24 of the A1 strand in PapA. In the PapGIIp, PapF, and PapK structures, the amino acid backbone of the A1 strand is approximately 2.4 Å further away, accommodating a 90° rotation of the PapD residue Ile105. Five water molecules are present around Leu107 in the PapD-GIIp structure, in accordance with other PapD-pilin structures, while the pockets surrounding the other G1-strand hydrophobic residues are dehydrated in the GIIp and all other structures. The relative plasticity of the P2 pocket of different pilin domains that interact with Leu107 of PapD may explain why mutants with mutations at position 107 can still assemble pili but mutants with mutations at position 105 cannot. The P2 pocket in the published PapD-PapA-PapA complex is unoccupied due to truncation of the Nte (63), making comparison of chaperone- and Nte-bound pilin domains difficult with respect to the P2-P4 pockets.

The PapD-GIIp complex exhibits an open, flexible P5 pocket. *In vitro*, the rate of DSE has been shown to be the slowest between PapG and the N-terminal extension of PapF, with a time to 50% completion (t_{50}) of approximately 120 h (51). PapF, which has an obstructed P5 pocket (Fig. 2F), undergoes DSE with a t_{50} of 76 h, while other pilin domains have much higher rates of exchange, with t_{50} values ranging from 3.2 to 12.5 h *in vitro* (65). In contrast, PapH does not undergo DSE, as its P5 pocket is completely obstructed (64) (Fig. 2E). It has been proposed that, *in vivo*, the rates of DSE are related to the openness of the P5 pocket (64).

The PapD-GIIp structure, therefore, is remarkable for exhibiting an open conformation of the P5 pocket in both form 1 and form 2 crystals (Fig. 2A and B). The P5 pocket is a hydrophobic pocket flanked by the E-F loop (residues 210 to 215, contributing Leu211) and the A2-B loop (residues 301 to 304, contributing Leu305) and backed by Tyr261, Leu257, and Leu293. Residues 210 to 215 of PapGIIp form 1, which comprise the E-F loop (Fig. 2A), exhibit relatively weak electron density, but a predominant conformation of this loop is stabilized by a crystal contact between Ile213 and a hydrophobic pocket of a symmetry-related copy of PapGIIp formed by Trp279 and Tyr280. Weak backbone electron density extends from Ile213, suggesting that a minor conformation of this loop that would put loop E-F in closer apposition to loop A2-B, leading to a conformation similar to that seen in form 2. Asp210 of form 2 makes a 2.75-Å hydrogen bond with Lys281 of a symmetry-related copy of GIIp, bringing Tyr280 of the symmetry-related molecule into a conformation that sterically excludes

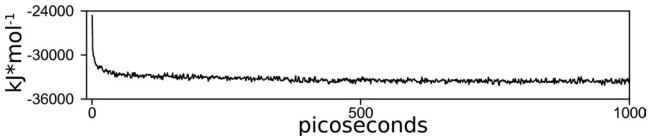

FIG 3 Total system energy over the 1,000-ps molecular dynamics simulation of the PapF-PapGII complex.

the conformation of Ile213 seen in form 1. In both crystal forms, the P5 pocket is in an open, solvent-exposed configuration that should be easily accessible to an incoming donor strand (Fig. 2A and B).

In order to assess the accessibility of the P5 pocket in PapGIIp to an incoming PapF Nte, we performed molecular dynamics simulations of the PapD-GIIp (form 1) complex. Placement of the P1 to P5 residues of the Nte of PapF for the initial model was done by superposition with the pilin domains in the published PapD-PapA-PapA complex (63) and mutation in COOT (13). A 1-ns simulation rapidly reached an energy minimum (Fig. 3), with the E-F loop collapsing on the PapF Nte with only a small shift toward the P5 pocket (Fig. 2D).

Next, to test the availability of the P5 pocket while the PapGIIp is in complex with PapD, the form 1 crystal structure was subjected to a 20-ns molecular dynamics simulation to assess the movement of the E-F and A2-B loops around the P5 pocket. In this simulation, Ile211, removed from crystal contacts, initially swings into close apposition with the A2-B loop (Fig. 4B), leading to a conformation in which the P5 pocket is essentially closed. At ~12 ns, PapGIIp reverts to an open conformation of the A2-B loop as Ile211 swings back out to assume a position similar to that in the crystal structure. This open conformation is maintained through the end of the simulation (Fig. 4C) in the absence of crystal contacts, suggesting plasticity around the P5 pocket and functional significance of the predominant conformation seen in the crystal structure.

To estimate the flexibility of the E-F and A2-B loops from our experimental diffraction data, we carried out automated TLS refinement of the form 1 and form 2 structures using the TLSMD server (44). TLS refinement of form 1 with six TLS groups identified, at an isoprobability magnitude of 85%, a purely translational displacement of 1.7 Å in a group representing the E-F loop (residues 211 to 217) and a screw displacement producing a maximal excursion of ~2.5 Å centered at Ile300 of the A2-B loop. Analysis of form 2 using the same number of groups (7) identifies an E-F loop group (residues 204 to 224) with a purely translational displacement of 1.3 Å and an identical screw displacement producing a maximal excursion of ~2.5 Å at Ile300 of the A2-B loop. These results provide experimental support for both the magnitude and direction of the approximately 6-Å shift between open and closed states in the PapD-GIIp molecular dynamics simulation (Fig. 4D). This analysis provides evidence, derived from simulation and directly from the crystallographic data, that the A2-B and E-F loops surrounding the P5 pocket of PapGIIp are highly flexible. Accessibility of the P5 pocket of PapGIIp is not likely to be a rate-limiting factor in DSE, as demonstrated by the ease of docking of the Nte of PapF into the crystallographic conformation of PapGIIp.

DISCUSSION

PapGII is found in the majority of *E. coli* isolates causing human clinical pyelonephritis, likely due to the ability of its adhesin domain to bind the globoside (GbO_4) expressed on human kidney epithelium (11). The intact PapD-GII chaperone-adhesin complex serves as the initiator of P-pilus synthesis by binding to the usher, PapC (33, 66). Further, the PapGII pilin domain's relatively low rate of DSE allows priming of pilus assembly, which proceeds to completion once PapG and PapF have undergone DSE (51). This study completes the structural inventory of P-pilus pilin domains and provides further insight into the mechanisms by which DSE occurs.

Previous molecular dynamics studies of PapF have shown that flexibility (or the lack thereof in PapH) in the A2-B and E-F loops surrounding the P5 pocket correlates with the relative rates at which these pilin domains achieve DSE (65), implying that availability of the P5 pocket to attack by the incoming Nte is a rate-

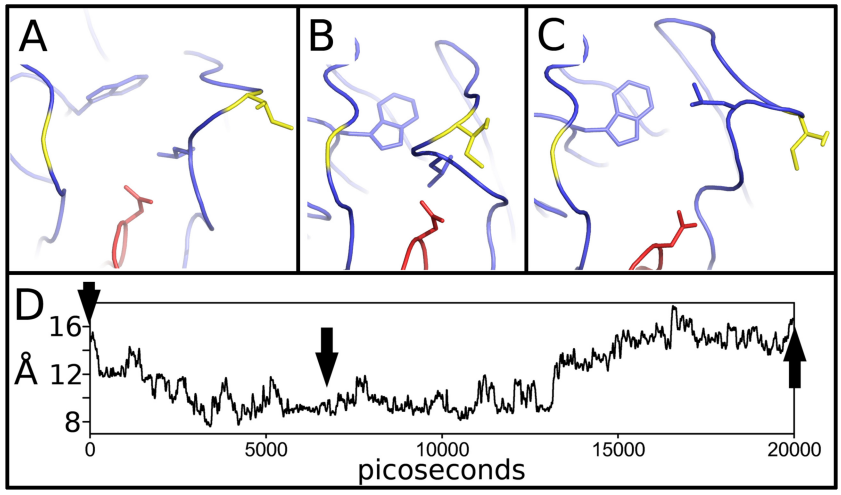

FIG 4 The distance between Gly323 (yellow, left) and Ile233 (yellow, right) of the PapGII (blue)-PapD (red) complex exhibits transient open and closed conformations represented by the crystallographic form 1 structure (A) and the simulated structure at 6 ns (B) and 20 ns (C). Trp281, which lies at the back of the P5 pocket, is shown in blue at center. (D) Distance between G323 and I233 over the entire simulation, with the structures in panels A to C indicated by arrows.

limiting step in DSE. This study builds on these results by showing that PapGIIp, the slowest of the pilin domains to achieve DSE *in vitro*, exhibits flexibility around the P5 pocket that might imply a rate of DSE more similar to that of PapE, PapA, or PapK, each of which has a high rate of DSE and an open P5 pocket. The overall conformation of the E-F and A2-B loops in our crystal structures is likely to be similar to what may exist in a PapGIIp-PapF complex.

Furthermore, both within two different crystal forms and in a simulation in the absence of crystal contacts, the P5 pocket of PapGIIp appears to be open and available for DSE. The rate-limiting factor for DSE of the PapF Nte into the PapGIIp *in vitro* is therefore unlikely to be due to inaccessibility of the P5 pocket relative to that of other pilin domains. PapD-G has a high affinity for the P-pilus usher PapC relative to other chaperone-subunit complexes (10, 56, 66). It has been shown to bind to the NTD of PapC with a K_D (equilibrium dissociation constant) of 10^{-9} M (66). Likewise, there is a high affinity of the tip-associated adhesin of the type 1 pilus to its usher (41, 56). In light of the two PapD-GIIp crystal structures and the results of the molecular dynamics studies presented here, the slow DSE of PapGIIp *in vitro* (51) suggests that catalysis of DSE by PapC is likely to accelerate exchange to the rate seen *in vivo*, where pili assemble in minutes (26). Indeed, while a completely closed P5 pocket in the case of the terminator PapH (64) is likely to prevent DSE, a P5 pocket that fluctuates between the open and closed states on a nanosecond time scale should allow protein-protein interactions if subunits are found in close proximity and in a permissive orientation, e.g., at the usher. We therefore conclude, first, that the imperfect association between flexibility around the P5 pocket and the rate of DSE indicates an active role for PapC in pilus assembly. The recent structure of the PapC homologue FimD bound to the adhesin FimH (46) reveals that, after binding to the initial chaperone-adhesin complex, the usher is positioned to recruit the next chaperone-subunit complex (PapD-PapF in the P-pilus system) in an orientation that would facilitate rapid DSE. Catalysis of DSE by orientation at the usher may be the primary determinant of the rate of DSE during physiological pilus assembly. Second, comparison of the structures of PapD bound to every pilin domain in the Pap system does not reveal why individual Ntes show a strict preference for cognate binding partners, while PapD is able to accommodate a variety of binding partners. Structural comparison of these structures with the structures of donor-strand-exchanged pilin domains is necessary to fill this scientific gap.

ACKNOWLEDGMENTS

We gratefully acknowledge the assistance of Jay Nix at the Advanced Light Source with collection of anomalous dispersion data for the form 1 crystals.

This work was funded by NIH grant RO1-AI49950 to S.H.

REFERENCES

1. **Anderson GG, et al.** 2003. Intracellular bacterial biofilm-like pods in urinary tract infections. Science **301**:105–107.
2. **Baga M, Norgren M, Normark S.** 1987. Biogenesis of E. coli Pap pili: PapH, a minor pilin subunit involved in cell anchoring and length modulation. Cell **49**:241–251.
3. **Baga M, et al.** 1984. Nucleotide sequence of the papA gene encoding the Pap pilus subunit of human uropathogenic Escherichia coli. J. Bacteriol. **157**:330–333.
4. **Bann JG, Pinkner JS, Frieden C, Hultgren SJ.** 2004. Catalysis of protein folding by chaperones in pathogenic bacteria. Proc. Natl. Acad. Sci. U. S. A. **101**:17389–17393.
5. **Barnhart MM, et al.** 2000. PapD-like chaperones provide the missing information for folding of pilin proteins. Proc. Natl. Acad. Sci. U. S. A. **97**:7709–7714.
6. **Barnhart MM, Sauer FG, Pinkner JS, Hultgren SJ.** 2003. Chaperone-subunit-usher interactions required for donor strand exchange during bacterial pilus assembly. J. Bacteriol. **185**:2723–2730.
7. **Bingen-Bidois M, et al.** 2002. Phylogenetic analysis and prevalence of urosepsis strains of Escherichia coli bearing pathogenicity island-like domains. Infect. Immun. **70**:3216–3226.
8. **Choudhury D, et al.** 1999. X-ray structure of the FimC-FimH chaperone-adhesin complex from uropathogenic Escherichia coli. Science **285**:1061–1066.
9. **Clegg S.** 1982. Cloning of genes determining the production of mannose-resistant fimbriae in a uropathogenic strain of Escherichia coli belonging to serogroup O6. Infect. Immun. **38**:739–744.
10. **Dodson KW, Jacob-Dubuisson F, Striker RT, Hultgren SJ.** 1993. Outer-membrane PapC molecular usher discriminately recognizes periplasmic chaperone-pilus subunit complexes. Proc. Natl. Acad. Sci. U. S. A. **90**:3670–3674.
11. **Dodson KW, et al.** 2001. Structural basis of the interaction of the pyelonephritic E. coli adhesin to its human kidney receptor. Cell **105**:733–743.
12. **Doublie S.** 2007. Production of selenomethionyl proteins in prokaryotic and eukaryotic expression systems. Methods Mol. Biol. **363**:91–108.
13. **Emsley P, Cowtan K.** 2004. Coot: model-building tools for molecular graphics. Acta Crystallogr. D Biol. Crystallogr. **60**:2126–2132.
14. **Gong M, Makowski L.** 1992. Helical structure of P pili from Escherichia coli. Evidence from X-ray fiber diffraction and scanning transmission electron microscopy. J. Mol. Biol. **228**:735–742.
15. **Griebling TL.** 2007. Urologic diseases in America, vol 07–5512. NIH, Washington, DC.
16. **Henderson NS, So SS, Martin C, Kulkarni R, Thanassi DG.** 2004. Topology of the outer membrane usher PapC determined by site-directed fluorescence labeling. J. Biol. Chem. **279**:53747–53754.
17. **Hess B, Kutzner C, van der Spoel D, Lindahl E.** 2008. GROMACS 4: algorithms for highly efficient, load-balanced, and scalable molecular simulation. J. Chem. Theor. Comput. **4**:435–447.
18. **Holmgren A, Branden CI.** 1989. Crystal structure of chaperone protein PapD reveals an immunoglobulin fold. Nature **342**:248–251.
19. **Hooton TM, Stamm WE.** 1997. Diagnosis and treatment of uncomplicated urinary tract infection. Infect. Dis. Clin. North Am. **11**:551–581.
20. **Hultgren SJ, Normark S, Abraham SN.** 1991. Chaperone-assisted assembly and molecular architecture of adhesive pili. Annu. Rev. Microbiol. **45**:383–415.
21. **Hung CS, et al.** 2002. Structural basis of tropism of Escherichia coli to the bladder during urinary tract infection. Mol. Microbiol. **44**:903–915.
22. **Hung DL, Knight SD, Hultgren SJ.** 1999. Probing conserved surfaces on PapD. Mol. Microbiol. **31**:773–783.
23. **Hung DL, Knight SD, Woods RM, Pinkner JS, Hultgren SJ.** 1996. Molecular basis of two subfamilies of immunoglobulin-like chaperones. EMBO J. **15**:3792–3805.
24. **Hung DL, Pinkner JS, Knight SD, Hultgren SJ.** 1999. Structural basis of chaperone self-capping in P pilus biogenesis. Proc. Natl. Acad. Sci. U. S. A. **96**:8178–8183.
25. **Jacob-Dubuisson F, Heuser J, Dodson K, Normark S, Hultgren S.** 1993. Initiation of assembly and association of the structural elements of a bacterial pilus depend on two specialized tip proteins. EMBO J. **12**:837–847.
26. **Jacob-Dubuisson F, Striker R, Hultgren SJ.** 1994. Chaperone-assisted self-assembly of pili independent of cellular energy. J. Biol. Chem. **269**:12447–12455.
27. **Jones CH, Danese PN, Pinkner JS, Silhavy TJ, Hultgren SJ.** 1997. The chaperone-assisted membrane release and folding pathway is sensed by two signal transduction systems. EMBO J. **16**:6394–6406.
28. **Jones CH, et al.** 1995. FimH adhesin of type 1 pili is assembled into a fibrillar tip structure in the Enterobacteriaceae. Proc. Natl. Acad. Sci. U. S. A. **92**:2081–2085.
29. **Justice SS, et al.** 2004. Differentiation and developmental pathways of uropathogenic Escherichia coli in urinary tract pathogenesis. Proc. Natl. Acad. Sci. U. S. A. **101**:1333–1338.
30. **Kabsch W.** 1978. A discussion of the solution for the best rotation to relate two sets of vectors. Acta Crystallogr. A **34**:827–828.
31. **Knight SD, et al.** 2002. Structure of the S pilus periplasmic chaperone

SfaE at 2.2 Å resolution. Acta Crystallogr. D Biol. Crystallogr. **58**:1016–1022.
32. **Kostakioti M, Newman CL, Thanassi DG, Stathopoulos C.** 2005. Mechanisms of protein export across the bacterial outer membrane. J. Bacteriol. **187**:4306–4314.
33. **Kuehn MJ, Heuser J, Normark S, Hultgren SJ.** 1992. P pili in uropathogenic E. coli are composite fibres with distinct fibrillar adhesive tips. Nature **356**:252–255.
34. **Kuehn MJ, et al.** 1993. Structural basis of pilus subunit recognition by the PapD chaperone. Science **262**:1234–1241.
35. **Lee YM, Dodson KW, Hultgren SJ.** 2007. Adaptor function of PapF depends on donor strand exchange in P-pilus biogenesis of Escherichia coli. J. Bacteriol. **189**:5276–5283.
36. **Leslie A.** 1992. Recent changes to the MOSFLM package for processing film and image plate data. *In* Joint CCP 4 + ESF-EAMCB newsletter on protein crystallography. no. 26.
37. **Lund B, Lindberg F, Normark S.** 1988. Structure and antigenic properties of the tip-located P pilus proteins of uropathogenic Escherichia coli. J. Bacteriol. **170**:1887–1894.
38. **Martinez JJ, Mulvey MA, Schilling JD, Pinkner JS, Hultgren SJ.** 2000. Type 1 pilus-mediated bacterial invasion of bladder epithelial cells. EMBO J. **19**:2803–2812.
39. **McCoy AJ, et al.** 2007. Phaser crystallographic software. J. Appl. Crystallogr. **40**:658–674.
40. **Mulvey MA, et al.** 1998. Induction and evasion of host defenses by type 1-piliated uropathogenic Escherichia coli. Science **282**:1494–1497.
41. **Munera D, Hultgren S, Fernandez LA.** 2007. Recognition of the N-terminal lectin domain of FimH adhesin by the usher FimD is required for type 1 pilus biogenesis. Mol. Microbiol. **64**:333–346.
42. **Nishiyama M, Ishikawa T, Rechsteiner H, Glockshuber R.** 2008. Reconstitution of pilus assembly reveals a bacterial outer membrane catalyst. Science **320**:376–379.
43. **Nuccio SP, Baumler AJ.** 2007. Evolution of the chaperone/usher assembly pathway: fimbrial classification goes Greek. Microbiol. Mol. Biol. Rev. **71**:551–575.
44. **Painter J, Merritt E.** 2006. TLSMD web server for the generation of multi-group TLS models. J. Appl. Crystallogr. **39**:109–111.
45. **Pellecchia M, Guntert P, Glockshuber R, Wuthrich K.** 1998. NMR solution structure of the periplasmic chaperone FimC. Nat. Struct. Biol. **5**:885–890.
46. **Phan G, et al.** 2011. Crystal structure of the FimD usher bound to its cognate FimC-FimH substrate. Nature **474**:49–53.
47. **Remaut H, et al.** 2006. Donor-strand exchange in chaperone-assisted pilus assembly proceeds through a concerted beta strand displacement mechanism. Mol. Cell **22**:831–842.
48. **Remaut H, et al.** 2008. Fiber formation across the bacterial outer membrane by the chaperone/usher pathway. Cell **133**:640–652.
49. **Roberts JA, Hardaway K, Kaack B, Fussell EN, Baskin G.** 1984. Prevention of pyelonephritis by immunization with P-fimbriae. J. Urol. **131**:602–607.
50. **Roberts JA, et al.** 1994. The Gal(alpha 1-4)Gal-specific tip adhesin of Escherichia coli P-fimbriae is needed for pyelonephritis to occur in the normal urinary tract. Proc. Natl. Acad. Sci. U. S. A. **91**:11889–11893.
51. **Rose RJ, et al.** 2008. Unraveling the molecular basis of subunit specificity in P pilus assembly by mass spectrometry. Proc. Natl. Acad. Sci. U. S. A. **105**:12873–12878.
52. **Sauer FG, et al.** 1999. Structural basis of chaperone function and pilus biogenesis. Science **285**:1058–1061.
53. **Sauer FG, Pinkner JS, Waksman G, Hultgren SJ.** 2002. Chaperone priming of pilus subunits facilitates a topological transition that drives fiber formation. Cell **111**:543–551.
54. **Sauer FG, Remaut H, Hultgren SJ, Waksman G.** 2004. Fiber assembly by the chaperone-usher pathway. Biochim. Biophys. Acta **1694**:259–267.
55. **Saulino ET, Bullitt E, Hultgren SJ.** 2000. Snapshots of usher-mediated protein secretion and ordered pilus assembly. Proc. Natl. Acad. Sci. U. S. A. **97**:9240–9245.
56. **Saulino ET, Thanassi DG, Pinkner JS, Hultgren SJ.** 1998. Ramifications of kinetic partitioning on usher-mediated pilus biogenesis. EMBO J. **17**:2177–2185.
57. **Sheldrick GM.** 2008. A short history of SHELX. Acta Crystallogr. A **64**:112–122.
58. **Slonim LN, Pinkner JS, Branden CI, Hultgren SJ.** 1992. Interactive surface in the PapD chaperone cleft is conserved in pilus chaperone superfamily and essential in subunit recognition and assembly. EMBO J. **11**:4747–4756.
59. **Soto GE, Hultgren SJ.** 1999. Bacterial adhesins: common themes and variations in architecture and assembly. J. Bacteriol. **181**:1059–1071.
60. **Striker R, Jacob-Dubuisson F, Freiden C, Hultgren SJ.** 1994. Stable fiber-forming and nonfiber-forming chaperone-subunit complexes in pilus biogenesis. J. Biol. Chem. **269**:12233–12239.
61. **Stromberg N, et al.** 1990. Host-specificity of uropathogenic Escherichia coli depends on differences in binding specificity to Gal alpha 1-4Gal-containing isoreceptors. EMBO J. **9**:2001–2010.
62. **Thanassi DG, Stathopoulos C, Dodson K, Geiger D, Hultgren SJ.** 2002. Bacterial outer membrane ushers contain distinct targeting and assembly domains for pilus biogenesis. J. Bacteriol. **184**:6260–6269.
63. **Verger D, Bullitt E, Hultgren SJ, Waksman G.** 2007. Crystal structure of the P pilus rod subunit PapA. PLoS Pathog. **3**:e73. doi:10.1371/journal.ppat.0030073.
64. **Verger D, Miller E, Remaut H, Waksman G, Hultgren S.** 2006. Molecular mechanism of P pilus termination in uropathogenic Escherichia coli. EMBO Rep. **7**:1228–1232.
65. **Verger D, et al.** 2008. Structural determinants of polymerization reactivity of the P pilus adaptor subunit PapF. Structure **16**:1724–1731.
66. **Volkan E, et al.** 2012. Domain activities of PapC usher reveal the mechanism of action of an Escherichia coli molecular machine. Proc. Natl. Acad. Sci. U. S. A. **109**:9563–9568.
67. **Waksman G, Hultgren SJ.** 2009. Structural biology of the chaperone-usher pathway of pilus biogenesis. Nat. Rev. Microbiol. **7**:765–774.
68. **Wright KJ, Seed PC, Hultgren SJ.** 2007. Development of intracellular bacterial communities of uropathogenic Escherichia coli depends on type 1 pili. Cell. Microbiol. **9**:2230–2241.
69. **Zavialov AV, et al.** 2003. Structure and biogenesis of the capsular F1 antigen from Yersinia pestis: preserved folding energy drives fiber formation. Cell **113**:587–596.
70. **Zavialov AV, Knight SD.** 2007. A novel self-capping mechanism controls aggregation of periplasmic chaperone Caf1M. Mol. Microbiol. **64**:153–164.